Disturbance/Uncertainty Estimator Based Integral Sliding-Mode Control

Burak Kürkçü, Coşku Kasnakoğlu, and Mehmet Önder Efe

***Abstract*—A disturbance/uncertainty estimator based integral sliding-mode control approach is introduced. Explicit mathematical expressions for robust stability, performance, and bandwidth requirement are derived. The integral sliding-mode controller is built to satisfy certain industrial criteria. It is integrated into the robustness analysis via its quasi-linear representation. The proposed methodology is experimentally verified on a high-precision gimbal control application. It is seen that the estimator works well and significantly improves performance and robustness in the presence of disturbances and uncertainties.**

***Index Terms*—Disturbance/uncertainty estimator (D/UE), gimbal control, integral sliding mode, robust stability (RS)/performance.**

I. Introduction

Sliding-mode control (SMC) is a nonlinear control technique that alters the dynamics of a system by application of a discontinuous control signal that forces the system to "slide" along a stable manifold. SMC methods date back to the 1950s [1] and have gained popularity and maturity since the 1970s [2]. Numerous successful applications and theoretical extension of SMC have taken place in the last decades, which include integral SMC (ISMC) [3] and time-varying sliding-surface design. [4]. SMC has also enjoyed success on nonlinear/time-delay systems [5] and systems lacking full-state measurements [6].

It is well established that the common SMC methods are insensitive against matched uncertainties and disturbances [7]. Unfortunately, this property is lost for unmatched disturbances [8], which include many practical systems where the uncertainties do not enter through the control channels [9]. A variety of control strategies, including a distributed active antidisturbance control [10] and linear matrix inequality (LMI)-based control [11], have been proposed to address the problems caused by the mismatched uncertainties.

Combining SMC or other control techniques with strategies that give estimates of uncertainties and disturbances has been a promising direction. The disturbance observer (DO) [or disturbance/uncertainty estimator (D/UE)] is one such strategy [12] together with its important extensions such as the modified uncertainty/disturbance estimator (MUDE) applicable to delayed systems [13]. Novel combinations of SMC and DO have been proposed including a method to construct sliding surfaces with disturbance estimation [14], the extension of this method to a larger class of disturbances [15] and to memoryless and memory-based integral sliding surfaces [16]. These studies also reveal that the ISMC handles mismatched uncertainties robustly and the DO alleviates chattering effects while retaining nominal performance.

A recent review collects major results in the literature regarding DO-based control (DOBC) [17]. Two research directions and open problems are identified as: "How to analyze the robust stability (RS) and performance for a designed DOBC strategy?" and "For a described level of uncertainty, how to develop a strategy that requires a minimum level of feedback or control bandwidth?"

These items constitute the main contribution of this study: Explicit expressions for RS, performance, and bandwidth requirements (specifically the overall control system bandwidth) are derived for a novel DOBC strategy. This is made possible by combining ISMC with an $\mathcal{H}_\infty$-controller embedded within the D/UE. As such, the D/UE has a unique form different from the usual Q-filter and plant inversion based architecture. Other contributions include the introduction of the total equivalent disturbance (TED) framework and experimental verification on an industrial gimbal system including comparison to state-of-the-art DOBC methodologies.

II. Disturbance/Uncertainty Estimator

A. Definition of Equivalent Input Disturbance (EID)

The concept of EID is reviewed briefly as it will help the development later. The general representation of an LTI system injected with a disturbance through an unknown channel $B_d d(t)$ is given as

$$\dot{x}_0(t) = Ax_0(t) + Bu(t) + B_d d(t), \quad y_0(t) = Cx_0(t) \tag{1}$$

where $A \in \mathbb{R}^{n\times n}$, $B \in \mathbb{R}^{n\times 1}$, $B_d \in \mathbb{R}^{n\times n_d}$, $C \in \mathbb{R}^{1\times n}$, $x_0(t) \in \mathbb{R}^{n\times 1}$, $y_0(t) \in \mathbb{R}$, $u(t) \in \mathbb{R}$, and $d(t) \in \mathbb{R}^{n_d\times 1}$. This case is called *mismatch condition* for $B \neq B_d$.

Assumption 1: (A, B, C) has no poles or zeros on the imaginary axis, the pair (A, B) is controllable, the pair (A, C) is observable and A has no eigenvalue in the right-half-plane.

Assumption 2: B is full column rank so that the psuedoinverse $B^+ := (B^T B)^{-1} B^T$ exists.

Let (X, Σ, μ) be a σ-finite measure space, over which L_1 denotes all integrable functions, i.e., $\int_X |f| d\mu < \infty$. Similarly L_∞ denotes all functions that are essentially bounded, i.e., $\exists M\ |f| \leq M < \infty$. This study deals with real functions defined almost everywhere so $f \in L_1$ simply means $\int_{\mathbb{R}} |f|\, dx < \infty$ and $f \in L_\infty$ means $\operatorname{ess\,sup}_{\mathbb{R}} |f| < \infty$.

Assumption 3: The disturbance of the system in (1) is bounded and integrable, i.e., $d \in L_1 \cap L_\infty$.

Remark 1: Assumption 1 is necessary to achieve output tracking. Assumption 2 guarantees the existence of B^+. Assumption 3 assures the integrability and boundedness of disturbances.

An equivalent LTI system, where disturbances enter only through the input channels, is given in

$$\dot{x}(t) = Ax(t) + B\left(u(t) + d_{\mathrm{ed}}(t)\right), \quad y(t) = Cx(t) \tag{2}$$

where $x(t) \in \mathbb{R}^{n\times 1}$, $y(t) \in \mathbb{R}$ and $d_{\mathrm{ed}}(t) := B^+ B_d d(t) \in \mathbb{R}$. This form is called the *matching condition* as d_{ed} is additive to u.

Manuscript received August 19, 2017; revised November 12, 2017; accepted February 3, 2018. Date of publication February 21, 2018; date of current version October 25, 2018. Recommended by Associate Editor X. Yu. *(Corresponding author: Coşku Kasnakoğlu.)*

B. Kürkçü is with ASELSAN Inc., Ankara 06172, Turkey, and also with the TOBB University of Economics and Technology, Ankara 06560, Turkey (e-mail: bkurkcu@etu.edu.tr).

C. Kasnakoğlu is with the TOBB University of Economics and Technology, Ankara 06560, Turkey (e-mail: kasnakoglu@etu.edu.tr).

M. Ö. Efe is with Hacettepe University, Ankara 06800, Turkey (e-mail: onderefe@hacettepe.edu.tr).

Color versions of one or more of the figures in this paper are available online at http://ieeexplore.ieee.org.

Digital Object Identifier 10.1109/TAC.2018.2808440

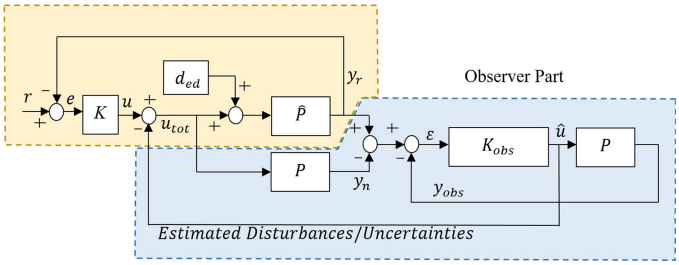

Fig. 1. Configuration of the overall proposed control system.

Definition 1: Consider the output y_0 of system (1) and the output y of system (2) under zero input $u \equiv 0$. The disturbance $d_{\rm ed}$ is called EID if $y_0(t) = y(t)$ for $\forall t \geq 0$.

Lemma 1 (see [18]): Under *Assumptions 1–3*, there always exists an EID satisfying *Definition 1*.

Based on the discussion in this section, the plant will be taken to be in the EID form (2) for the rest of this paper.

B. Disturbance/Uncertainty Estimator

The configuration for overall proposed estimator system is illustrated in Fig. 1, where K is the main controller, $K_{\rm obs}$ is the controller for the observer (i.e., D/UE), $\varepsilon(t) \in \mathbb{R}$ is the observer error, $u(t) \in \mathbb{R}$ is the output generated by the main controller, $\hat{u}(t) \in \mathbb{R}$ is the estimation of the D/UE. The proposed system includes two separate feedback loops: The top-left one is a unity-feedback system built via ISMC (K). The bottom-right one is the D/UE, within which the signal $\hat{u}$ is the estimated disturbances and uncertainties. The perturbed plant $\hat{P}$ is defined as

$$\hat{P} \in \{P(1 + \Delta W_T) \quad | \quad \forall \, \|\Delta\|_\infty \leq 1\} \tag{3}$$

where W_T denotes robustness weight function that is stable strictly proper and Δ is any unstructured uncertainty function. The nominal plant P can be represented as

$$P = C(sI - A)^{-1}B. \tag{4}$$

In the following, we establish some results based on Fig. 1, which will be used to analyze the behavior of the proposed D/UE-based control system.

Lemma 2: The estimation produced by the D/UE can be written in terms of the complementary sensitivity function of the observer part $T_{\rm obs} := 1 - S_{\rm obs} = PK_{\rm obs}(1 + PK_{\rm obs})^{-1}$ as

$$\hat{u} = T_{\rm obs}(\Delta W_T u_{\rm tot} + d_{\rm ed} + \Delta W_T d_{\rm ed}) \, . \tag{5}$$

Proof: From Fig. 1, one can write

$$y_r = \hat{P}(u_{\rm tot} + d_{\rm ed}), \quad y_n = Pu_{\rm tot}, \quad y_{\rm obs} = P\hat{u}. \tag{6}$$

$$\begin{aligned} \varepsilon &:= y_r - y_n - y_{\rm obs} = \hat{P}u_{\rm tot} - Pu_{\rm tot} + \hat{P}d_{\rm ed} - P\hat{u} \\ &= S_{\rm obs}(y_r - y_n) = S_{\rm obs}((\hat{P} - P)u_{\rm tot} + \hat{P}d_{\rm ed}). \end{aligned} \tag{7}$$

where $S_{\rm obs} = (1 + PK_{\rm obs})^{-1}$. Reorganizing (7) yields

$$P\hat{u} = T_{\rm obs}P(\Delta W_T u_{\rm tot} + d_{\rm ed} + \Delta W_T d_{\rm ed}) \tag{8}$$

and for $P \neq 0$ this implies (5). ■

Remark 2: Due to Assumption 1, it is possible to design $K_{\rm obs}$ such that $\varepsilon(t) \to 0$ in the desired frequency range. This design will be carried out in Section III-A via $\mathcal{H}_\infty$-control. Lemma 2 states that the estimation of the disturbances/uncertainties depend on the sensitivity function of observer part, i.e., $S_{\rm obs}$ (or $T_{\rm obs}$). By shaping this function, one can control various estimation characteristics. For instance, one can adjust the bandwidth by having $T_{\rm obs}(j\omega) \approx 1$ for frequencies, where full estimation is desired. As another example, if no overshoot in estimation is desired, one can impose $\|T_{\rm obs}\|_\infty \leq 1$.

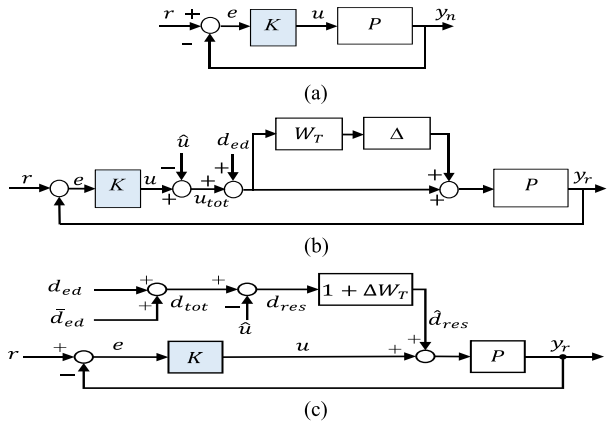

Fig. 2. Block diagrams of the nominal and perturbed systems. (a) Nominal system. (b) Perturbed system. (c) TED form of the perturbed system.

C. Total Equivalent Disturbance

A consequence of Lemma 2 is that the D/UE estimates a signal of the form (5), which is not only the disturbance $d_{\rm ed}$ but also some effect brought upon by the uncertainty ΔW_T. Thus, from the viewpoint of the estimator, the effective disturbance is more than just $d_{\rm ed}$, which we formalize in this section.

Definition 2: Consider the nominal system in Fig. 2 (a) and the perturbed system subject to disturbance $d_{\rm ed}$ in Fig. 2(b). The *TED* is defined as

$$d_{\rm tot} = \bar{d}_{\rm ed} + d_{\rm ed} \tag{9}$$

where

$$\bar{d}_{\rm ed} = (1 + \Delta W_T)^{-1}\Delta W_T u \, . \tag{10}$$

The *residual disturbance* $d_{\rm res}$ is defined as the difference between the total disturbance $d_{\rm tot}$ and the estimation $\hat{u}$, i.e., $d_{\rm res} = d_{\rm tot} - \hat{u}$. Finally, the *perturbed residual disturbance* is defined as

$$\hat{d}_{\rm res} = (1 + \Delta W_T)d_{\rm res} \, . \tag{11}$$

Lemma 3: Under Definition 2, the perturbed system in Fig. 2(b) and the alternative form in Fig. 2(c) are equivalent.

Proof: Clearly Fig. 2(b) and (c) would be equivalent if a given input produces the same y_r in both cases. For Fig. 2(b)

$$y_r = P(1 + \Delta W_T)(u_{\rm tot} + d_{\rm ed}) \, . \tag{12}$$

From the block diagram in Fig. 2(c) and using Definition 2

$$\begin{aligned} y_r &= Pu + P(1 + \Delta W_T)(1 + \Delta W_T)^{-1}\Delta W_T u \\ &\quad + P(1 + \Delta W_T)(d_{\rm ed} - \hat{u}) = P(1 + \Delta W_T)(u + d_{\rm ed} - \hat{u}) \end{aligned}$$

from where (12) follows. ■

The TED concept allows restructuring Lemma 2 into the following theorem.

Theorem 1: The estimation produced by the D/UE is

$$\hat{u} = T_{\rm obs}(1 + \Delta W_T)(1 + T_{\rm obs}\Delta W_T)^{-1}d_{\rm tot}. \tag{13}$$

Proof: Rewriting (5) with $u_{\rm tot} = u - \hat{u}$ yields

$$\hat{u} = T_{\rm obs}(\Delta W_T(u - \hat{u}) + d_{\rm ed} + \Delta W_T d_{\rm ed}).$$

Grouping terms with $\hat{u}$

$$(1 + T_{\rm obs}\Delta W_T)\hat{u} = T_{\rm obs}(\Delta W_T u + (1 + \Delta W_T)d_{\rm ed})\ .$$

Solving for $\hat{u}$, we obtain

$$\begin{aligned}\hat{u} &= T_{\rm obs}\bar{D}(\Delta W_T u + (1 + \Delta W_T)d_{\rm ed}) \\ &= T_{\rm obs}(1 + \Delta W_T)\bar{D}((1 + \Delta W_T)^{-1}\Delta W_T u + d_{\rm ed})\end{aligned}$$

where $\bar{D} := (1 + T_{\rm obs}\Delta W_T)^{-1}$. Utilizing Definition 2 yields

$$\hat{u} = T_{\rm obs}(1 + \Delta W_T)\bar{D}(\bar{d}_{\rm ed} + d_{\rm ed}) = T_{\rm obs}(1 + \Delta W_T)\bar{D}d_{\rm tot}.$$

■

The theorem states that the performance of the estimator depends tightly on the bandwidth of the estimator ($\omega_{\rm obs}$) expressed in the following equivalent forms:

$$\text{Within the BW} \Leftrightarrow T_{\rm obs} \approx 1 \Leftrightarrow S_{\rm obs} \approx 0 \Leftrightarrow \omega \ll \omega_{\rm obs} \tag{14}$$

$$\text{Out of the BW} \Leftrightarrow T_{\rm obs} \approx 0 \Leftrightarrow S_{\rm obs} \approx 1 \Leftrightarrow \omega \gg \omega_{\rm obs} \tag{15}$$

$$\text{Transition} \Leftrightarrow T_{\rm obs}, S_{\rm obs} \not\approx \{0, 1\} \Leftrightarrow \omega \text{ close to } \omega_{\rm obs}. \tag{16}$$

Based on these comments and Theorem 1, the following remark is useful.

Remark 3: Within its bandwidth, the D/UE perfectly estimates the total disturbance since $\hat{u} = d_{\rm tot}$ if $T_{\rm obs} = 1$. From Fig. 2(c), it is clear that $\hat{d}_{\rm res} = (1 + \Delta W_T)d_{\rm res} = 0$. In this case, Fig. 2(c) reduces to (a). So within its bandwidth, the D/UE makes the perturbed system behave as the nominal system. Outside its bandwidth, the estimate of the D/UE is zero since $\hat{u} = 0$ for $T_{\rm obs} = 0$. Thus, the system behaves as if there was no D/UE.

III. Controller Design

The main task of control system design is to satisfy the robust performance objective. For robust performance, the following two expressions must hold true at the same time

$$\|W_T T\|_\infty < 1 \quad \text{and} \quad \|W_P \hat{P}\hat{S}\|_\infty < 1 \tag{17}$$

where W_P is the performance weight, $S = (1 + PK)^{-1}$ is the sensitivity function, $T = PK(1 + PK)^{-1}$ is the complementary sensitivity function, and $\hat{S}$ is the sensitivity function for all possible plants ($\hat{S} = (1 + \hat{P}K)^{-1}$). The first equality in (17) by itself is the RS criterion [19].

A. Design Procedure for $K_{\rm obs}$ Using $\mathcal{H}_\infty$ Control

This synthesis of $K_{\rm obs}$ is based on the model-matching approach that is defined in [19]. The model matching problem is to find the minimum model-matching error for

$$\gamma_{\rm opt} := \min_{Q_{\rm im}} \|T_1 - T_2 Q_{\rm im}\|_\infty \tag{18}$$

where $Q_{\rm im}$ is a stable yet possibly improper transfer function that satisfies (18) and $T_1, T_2 \in \Omega$, where Ω denotes the family of all stable, proper, and real-valued rational transfer functions. In addition, T_2 should have no zeros on the imaginary axis. As seen in Fig. 1, $K_{\rm obs}$ only acts on the nominal plant P. Since estimation of high-frequency disturbances/uncertainties are not of interest, the output of $K_{\rm obs}$ should be shaped by a weighing function W_U. Thus, the robust performance criterion for designing $K_{\rm obs}$ is rearranged as

$$\| |W_P S_{\rm obs}|^2 + |W_U K_{\rm obs} S_{\rm obs}|^2 \|_\infty < 1/2 \tag{19}$$

where W_U is the control input weight. A coprime factorization for $S_{\rm obs}$ and $T_{\rm obs}$ exists as

$$S_{\rm obs} = M(Y - NQ), \quad T_{\rm obs} = N(X + MQ) \tag{20}$$

where X, Y, M, and N are polynomials used in the coprime factorization of the plant. Q is any function belonging to Ω. After the performance weight W_P, control input weight W_U and the nominal plant are defined, the control system design procedure is carried out in the following steps:

1) First, the coprime factorization of plant is obtained.
2) A transfer function $Q_{\rm im}$ that minimizes the modified robust performance problem

$$\| |W_P M(Y - NQ_{\rm im})|^2 + |W_U M(X + MQ_{\rm im})|^2 \|_\infty < 1/2$$

is obtained. This expression can be simplified by defining

$$\begin{aligned} R_1 &:= W_P MY, \quad R_2 := W_P MN \\ S_1 &:= W_U MX, \quad S_2 := W_U MM \end{aligned} \tag{21}$$

which yields

$$\| |R_1 - R_2 Q_{\rm im}|^2 + |S_1 - S_2 Q_{\rm im}|^2 \|_\infty < 1/2. \tag{22}$$

3) Equation (22) is a quadratic function of $Q_{\rm im}$. To employ the model-matching algorithm, (22) needs to be transformed into the following form

$$\| |U_1 - U_2 Q_{\rm im}|^2 + U_3 \|_\infty < 1/2 \tag{23}$$

where U_1 and U_2 are stable, proper, real-rational transfer functions, and U_3 is a real-rational transfer function with $\overline{U}_3 = U_3$, where $\overline{U}_3$ denotes $U_3(-s)$. The functions U_1 and U_2 can be expanded as follows:

$$U_1 := (\overline{R}_2 R_1 + \overline{S}_2 S_1)\overline{F}_{\rm sf}^{-1} V_{\rm ap}, U_2 =: F_{\rm sf} V_{\rm ap} \tag{24}$$

where $F_{\rm sf}$ denotes the spectral factor of the function $F := \overline{R}_2 R_2 + \overline{S}_2 S_2$. In addition, F has no zeros or poles on the imaginary axis, $\overline{F} = F$ and $F(0) > 0$. $V_{\rm ap}$ denotes an arbitrary all-pass function such that $U_1 \in \Omega$. The function U_3 is in the form

$$U_3 = (\overline{W}_P W_P \overline{W}_U W_U)(\overline{W}_P W_P + \overline{W}_U W_U)^{-1} \tag{25}$$

where $\overline{W}_P$ denotes $W_P(-s)$ and $\overline{W}_U$ denotes $W_U(-s)$. If $\|U_3\|_\infty \geq 0.5$, the model-matching problem is not solvable.
4) The final model-matching problem can be obtained from (23) as

$$\|{U_4}^{-1} U_1 - {U_4}^{-1} U_2 Q_{\rm im}\|_\infty < 1, \ \forall \omega \tag{26}$$

where U_4 denotes a spectral factor of $\frac{1}{2} - U_3$.
5) With $T_1 := {U_4}^{-1} U_1, T_2 := {U_4}^{-1} U_2$, inequality (26) is of the form (18), which can be solved for $Q_{\rm im}$.
6) It must be checked that $Q_{\rm im}$ and the final form of Q are proper. If not, one can multiply $Q_{\rm im}$ with a suitable low-pass filter to satisfy $\|T_1 - T_2 Q\|_\infty < 1$.
7) The controller $K_{\rm obs}$ is obtained for internal stability through Youla–Kucera parameterization

$$K_{\rm obs} = (X + MQ)/(Y - NQ). \tag{27}$$

The design procedure described by the above-mentioned steps usually produces a satisfactory solution. However, the resulting controller is generally high order, which might cause difficulties in physical implementation. Some model reduction techniques could be useful at this point.

B. ISMC Design for K

The reference tracking problem using integral sliding mode (ISMC) is now considered. The controller design is performed utilizing the equivalent disturbance form of the system in Fig. 2(c). Note that the D/UE already cancels the disturbances in a target frequency range, easing the workload of the ISMC. Some residuals may still remain, however, especially at higher frequencies, as well as disturbances/uncertainties not captured by the EID [14]. In this fashion, the D/UE and ISMC complement each other in an overlapping way, possibly creating some redundancy desirable in critical industrial/military systems.

Let the transfer function of the plant be

$$\alpha \frac{B(s)}{A(s)} = \alpha \frac{s^m + b_1 s^{m-1} + \cdots + b_m}{s^n + a_1 s^{n-1} + \cdots + a_n} \tag{28}$$

with $n < m$ and $r = n - m$ being the *relative degree*. The system can be written in normal form

$$\begin{aligned} \dot{z} &= B_n z + P_n \zeta_1, \quad \dot{\zeta}_i = \zeta_{i+1}, \quad i = 1, \ldots, r-1 \\ \dot{\zeta}_r &= R_n z + S_n \zeta + \alpha u, \quad y = \zeta_1 \end{aligned} \tag{29}$$

where the subscript n stands for normal form and

$$\zeta := [\zeta_1, \ldots, \zeta_r]^T = [y, \dot{y}, \ldots, y^{(r-1)}]^T.$$

Assumption 4: Without loss of generality, we assume $\alpha > 0$; if not, one can redefine $\alpha \leftarrow -\alpha$ and $u \leftarrow -u$, which leaves (29) unchanged.

Assumption 5: The system (29) is assumed to be *minimum phase* for the output tracking to be possible. (Exact tracking of the output is not possible if the assumption fails, though acceptable results may still be possible.)

The form (29) can be viewed as an interconnection of two blocks. The z-system is called the *zero dynamics*. This system has input $y = \zeta_1$ and is stable due to Assumption 1. Thus, the control design effort can be concentrated on the ζ-system. The perturbed ζ-system can be expressed compactly as

$$\zeta^{(r)} = f + \alpha \left(u + \hat{d}_{\text{res}} \right), \quad y = \zeta_1 \tag{30}$$

where $f := f(z, \zeta) = R_n z + S_n \zeta$ and $\hat{d}_{\text{res}}$ is a matched disturbance as shown in Fig. 2(c). The sliding manifold is defined in operator notation as

$$\sigma := (\mathbf{D} + \lambda)^r (e_I) \tag{31}$$

where $\lambda > 0$, $\mathbf{D} := \frac{d}{dt}$, $e_I := \int e$, $e := y - y_d = \zeta_1 - y_d$, and y_d is the desired trajectory. The definition of (31) that on the sliding surface imposes, i.e., for $\sigma = 0$, e_I and its derivatives (including $e = y - y_d$) converge asymptotically to achieve $y \to y_d$.

The initial state $e_I(0)$ of the integrator element can be tailored to start the system directly on the sliding manifold at $t = 0$ and this removes the reaching phase. This is desirable as the system is more susceptible to noises and uncertainties during this phase [3].

Theorem 2: Let the sliding manifold σ be defined as in (31). Let the integrator initial condition be

$$e_I(0) = -\sum_{k=0}^{r-1} \binom{r}{k+1} \lambda^{-k-1} e^{(k)}(0). \tag{32}$$

where $\binom{r}{k+1}$ is the binomial coefficient indexed by r and $k+1$. Then, $\sigma(0) = 0$.

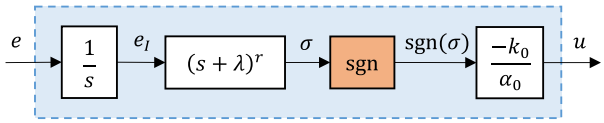

Fig. 3. Inner structure of the ISMC block K.

Proof: The sliding manifold σ in (31) can be written as

$$\sigma = (\mathbf{D} + \lambda)^r (e_I) = \sum_{k=0}^{r} \binom{r}{k} \lambda^{r-k} e_I^{(k)}.$$

At $t = 0$

$$\begin{aligned} \sigma(0) &= \lambda^r e_I(0) + \sum_{k=1}^{r} \binom{r}{k} \lambda^{r-k} e_I^{(k)}(0) \\ &= \lambda^r e_I(0) + \sum_{k=0}^{r-1} \binom{r}{k+1} \lambda^{r-k-1} e^{(k)}(0). \end{aligned}$$

Equating to zero and solving for $e_I(0)$

$$e_I(0) = -\lambda^{-r} \left(\sum_{k=0}^{r-1} \binom{r}{k+1} \lambda^{r-k-1} e^{(k)}(0) \right)$$

from which (32) follows directly. ■

The time derivative of the sliding manifold (31) is

$$\dot{\sigma} = (\mathbf{D} + \lambda)^r e = \sum_{k=0}^{r} \binom{r}{k} \lambda^{r-k} e^{(k)} \tag{33}$$

$$= y^{(r)} - y_d^{(r)} + \sum_{k=0}^{r-1} \binom{r}{k} \lambda^{r-k} e^{(k)} \tag{34}$$

$$= f + \alpha \left(u + \hat{d}_{\text{res}} \right) - y_d^{(r)} + \sum_{k=0}^{r-1} \binom{r}{k} \lambda^{r-k} e^{(k)}. \tag{35}$$

The ideal input choice to achieve $\dot{\sigma} = 0$ would be

$$u_{\text{ideal}} = -\hat{d}_{\text{res}} + \frac{1}{\alpha} \left(-f + y_d^{(r)} - \sum_{k=0}^{r-1} \binom{r}{k} \lambda^{r-k} e^{(k)} \right) \tag{36}$$

but this input may not be used directly, because of the following practical limitations related to industrial systems.

1) The perturbed residual disturbance $\hat{d}_{\text{res}}$ is unknown. In addition, while the plant uncertainties are ideally absorbed into $\hat{d}_{\text{res}}$, in practice some residuals may remain. Hence, differences may arise between the actual values of α and f and those used in the controller (i.e., those of the nominal plant). We denote the latter by α_0 and f_0.
2) In certain applications, it may be infeasible to modify the controller block structure in Fig. 1. That is, only the tracking error $e = y - y_d$ is fed to the controller and no additional information (e.g., plant states, reference signal) can be utilized (Derivatives of the error $e^{(k)}$ are required to compute the sliding surface σ but it is possible to obtain these from e using robust differentiation methods [20] or bandlimited differentiation as described in the following section.).

Theorem 3: The following control law with the block diagram given in Fig. 3 achieves tracking of y_d under both constraints 1 and 2 listed earlier:

$$u = -\frac{k_0}{\alpha_0} \text{sgn}(\sigma) \tag{37}$$

where

$$k_0 > \alpha^+ f^+ + \alpha_0 d^+ + \alpha^+ y_d^+ + \alpha^+ u^+ + \alpha^+ \eta \tag{38}$$

and

$$\alpha_0/\alpha < \alpha^+, \quad |f| < f^+, \quad |\hat{d}_{\text{res}}| < d^+, \quad |y_d^{(r)}| < y_d^+,$$
$$\left| \sum_{k=0}^{r-1} \binom{r}{k} \lambda^{r-k} e^{(k)} \right| < u^+, \quad \eta > 0. \tag{39}$$

Proof: Defining $V = \frac{1}{2}\sigma^2$ and differentiating

$$\dot{V} = \dot{\sigma}\sigma = \left(f + \alpha \left(u + \hat{d}_{\text{res}} \right) - y_d^{(r)} + \bar{U} \right) \sigma$$

where $\bar{U} := \sum_{k=0}^{r-1} \binom{r}{k} \lambda^{r-k} e^{(k)}$. Substituting (37)

$$\dot{V} = f\sigma + \alpha \hat{d}_{\text{res}} \sigma - y_d^{(r)} \sigma + \bar{U}\sigma - \frac{\alpha}{\alpha_0} k_0 |\sigma|.$$

To achieve $\dot{V} = \dot{\sigma}\sigma < -\eta|\sigma|$ for a given $\eta > 0$, it must hold that

$$k_0 > \frac{\alpha_0}{\alpha} \left| f + \alpha \hat{d}_{\text{res}} - y_d^{(r)} + \bar{U} \right| + \frac{\alpha_0}{\alpha} \eta.$$

Using triangle inequality, a higher bound can be obtained; so choosing k_0 as in the following equation will satisfy the above-mentioned condition

$$k_0 > \frac{\alpha_0}{\alpha} |f| + \alpha_0 \left| \hat{d}_{\text{res}} \right| + \frac{\alpha_0}{\alpha} \left| y_d^{(r)} \right| + \frac{\alpha_0}{\alpha} |\bar{U}| + \frac{\alpha_0}{\alpha} \eta.$$

Using the bounds defined in (39), it is clear that one can choose k_0 as defined in (38) to satisfy the above-mentioned expression. Hence, follows the statement of the theorem. ■

Remark 4: At this point, it is useful to note once again how the D/UE improves the ISMC design. If good estimates are provided for disturbances/uncertainties, the bounds α^+, d^+ will be small. From (38), this enables using a smaller gain for k_0. This reduces the switching gain of the ISMC, alleviating high-gain related problems, such as chattering. A similar approach has been employed in [14].

C. Quasi-Linear Representation of the System

The describing function $N(A^*, s)$ for a nonlinear system is essentially the equivalent of frequency response but it can depend on both the amplitude and frequency of an input sinusoid $A^* \sin(\omega t)$. The frequency domain representation of the sliding-mode controller (37) with block diagram shown in Fig. 3 can be expressed as

$$U(A^*, s) = -\frac{k_0}{\alpha_0} N(A^*, s) \sigma(s) \tag{40}$$

where $N(A^*, s)$ is the describing function of the nonlinearity, i.e., the signum function. From (31)

$$\sigma(s) = (s+\lambda)^r E_I(s) = (s+\lambda)^r \frac{E(s)}{s}. \tag{41}$$

Substituting (41) into (40) yields

$$U(A^*, s) = -\frac{k_0}{\alpha_0} N(A^*, s) (s+\lambda)^r \frac{E(s)}{s}. \tag{42}$$

The describing function of the signum function can be derived as in [21], which is

$$N(A^*, s) = N(A^*) = 4/(\pi A^*). \tag{43}$$

Substituting (43) into (42) gives the quasi-linear transfer function for the sliding-mode controller as

$$K(A^*, s) = -\frac{4k_0}{\pi A^* \alpha_0} \frac{(s+\lambda)^r}{s}. \tag{44}$$

To alleviate chattering, it is common to replace the sign function $\text{sgn}(\sigma)$ with $\text{sat}(\sigma/\phi)$, i.e., a saturation function with boundary layer thickness ϕ. Its describing function can be derived as in [21], which is

$$N(A^*) = \begin{cases} \frac{1}{\phi}, & A^* \le \phi \\ \frac{2}{\phi\pi} \left[\sin^{-1}\left(\frac{\phi}{A^*}\right) + \frac{\phi}{A^*} \sqrt{1 - \frac{\phi^2}{A^{*2}}} \right], & A^* > \phi \end{cases}. \tag{45}$$

Also, in addition to being highly sensitive to noise, the numerical differentiation in the definition of the sliding surface σ could result in an improper transfer function, which is problematic for implementation. For this reason, a bandlimited derivative is frequently employed, i.e.,

$$\sigma(s) = \left(\frac{s}{s/N_f + 1} + \lambda \right)^r E_I(s) \tag{46}$$

is used in place of (41) where $N_f > 0$. Substituting (45) and (46) into (40) and carrying out the computations yield

$$K(A^*, s) = \begin{cases} -\frac{k_0}{\alpha_0 \phi} K_1(s), & A^* \le \phi \\ -\frac{2k_0}{\alpha_0 \phi \pi} K_2(s), & A^* > \phi \end{cases} \tag{47}$$

where

$$K_1(s) = \frac{1}{s} \left(\frac{s}{s/N_f + 1} + \lambda \right)^r$$
$$K_2(s) = \left[\sin^{-1}\left(\frac{\phi}{A^*}\right) + \frac{\phi}{A^*} \sqrt{1 - \frac{\phi^2}{A^{*2}}} \right] K_1(s). \tag{48}$$

The quasi-linear transfer functions (44) and (47) can be thought of as a family of regular transfer functions parameterized by A^*. The frequency characteristics of the closed-loop system under the ISMC (37) can be obtained through multiple runs varying A^* within a range of interest. The importance of this approach is that the ISMC can be integrated into the frequency-domain RS/performance analysis to be carried out in the succeeding sections. To simplify the notation in the rest of the paper, we shall drop the arguments A^* and s and simply use K to denote the quasi-linear transfer function of the controller.

D. Robustness Improvement of the Proposed System

The proposed D/UE has important benefits against disturbances/uncertainties as captured by the following theorems.

Theorem 4: With the usage of proposed D/UE, the RS condition for the system is

$$\left\| W_T T \frac{S_{\text{obs}}}{1 - |W_T T_{\text{obs}}|} \right\|_\infty < 1. \tag{49}$$

Proof: Let $L_p = PK$ denote the loop transfer function for the nominal plant. For the design of K, the nominal closed-loop [see Fig. 2(a)] is also stable so the Nyquist plot for L_p does not encircle the point $-1 + j0$. Let $\hat{L}_p$ be the loop transfer function for the perturbed plant in Fig. 2(b). It is clear from Fig. 2(b) that $\hat{L}_p$ is indeed the transfer function from e to y_r, i.e.,

$$\hat{L}_p = \hat{P}K\bar{D} = PK + PKW_T S_{\text{obs}} \bar{D}\Delta$$

where $\bar{D} = (1 + T_{\rm obs}\Delta W_T)^{-1}$. Since the set of all possible plants is norm-bounded, following statements must hold for RS:

$$\begin{aligned} \text{RS} &\Leftrightarrow |1 + \hat{L}_p| \neq 0 \quad \Leftrightarrow \quad |1 + \hat{L}_p| > 0 \\ &\Leftrightarrow \quad \left|1 + PK + PKW_T S_{\rm obs}\bar{D}\Delta\right| > 0 \end{aligned}$$

for all ω, $\hat{L}_p$, and Δ. For the worst case, Δ is such that the magnitude is $|\Delta| = 1$ and the phase is such that the terms $1 + PK$ and $PKW_T S_{\rm obs}\bar{D}\Delta$ have opposite signs. Thus

$$\begin{aligned} \text{RS} &\Leftrightarrow |1 + PK| - \left|PKW_T S_{\rm obs}\bar{D}\right| > 0 \quad \forall\omega \\ &\Leftrightarrow \left|W_T S_{\rm obs}\bar{D}T\right| < 1 \quad \forall\omega \qquad (50) \\ &\Leftrightarrow \left|\frac{W_T S_{\rm obs}}{1 + T_{\rm obs}\Delta W_T}T\right| < 1 \quad \forall\omega. \qquad (51) \end{aligned}$$

To simplify further, note that

$$1 \leq |1 + \Delta W_T T_{\rm obs}| + |W_T T_{\rm obs}| \quad \forall\omega \qquad (52)$$

and therefore

$$1 - |W_T T_{\rm obs}| \leq |1 + \Delta W_T T_{\rm obs}| \quad \forall\omega \qquad (53)$$

$$\left|\frac{W_T S_{\rm obs}}{1 + T_{\rm obs}\Delta W_T}\right| \leq \left|\frac{W_T S_{\rm obs}}{1 - |W_T T_{\rm obs}|}\right| \quad \forall\omega. \qquad (54)$$

Using this final expression, it is clear that (51) holds if

$$\left|\frac{W_T S_{\rm obs}}{1 - |W_T T_{\rm obs}|}T\right| < 1 \quad \forall\omega$$

which is the statement of the theorem. ■

Theorem 5: With the use of the proposed D/UE, the robust performance condition is

$$\left\|\frac{W_P \hat{P} S S_{\rm obs}}{1 - |W_T T_{\rm obs}|}\right\|_\infty < 1. \qquad (55)$$

Proof: The robust performance goal can be posed as minimizing the effect of the disturbance on the output [19]. From the block diagram in Fig. 2(c), one obtains the transfer function from $D_{\rm tot}$ to Y_r as

$$Y_r/D_{\rm res} = P(1 + \Delta W_T)/(1 + PK) = \hat{P}S. \qquad (56)$$

Expressing in terms of amplitude

$$|Y_r| = |\hat{P}SD_{\rm res}| = |\hat{P}S(D_{\rm tot} - \hat{U})|. \qquad (57)$$

From Theorem 1

$$|Y_r| = \left|\hat{P}S(1 - T_{\rm obs}(1 + \Delta W_T)\bar{D})D_{\rm tot}\right| = \left|\hat{P}SS_{\rm obs}\bar{D}D_{\rm tot}\right|$$

where $\bar{D} = (1 + T_{\rm obs}\Delta W_T)^{-1}$. Arranging and weighing the error with W_P

$$|(W_P Y_r)/D_{\rm tot}| = \left|(W_P \hat{P} S S_{\rm obs})/(1 + T_{\rm obs}\Delta W_T)\right| \qquad (58)$$

and requiring the expression to be less than unity for all frequencies imply

$$\left|W_P \hat{P} S S_{\rm obs}\bar{D}(j\omega)\right| < 1 \ \ \forall\omega \in \mathbb{R}, \forall\Delta. \qquad (59)$$

By the help of (52) and (53)

$$\left|\frac{W_P \hat{P} S S_{\rm obs}}{1 - |T_{\rm obs}W_T|}(j\omega)\right| < 1 \ \ \forall\omega \in \mathbb{R}, \forall\Delta \qquad (60)$$

which justifies (55). ■

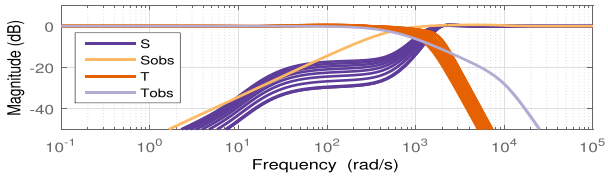

Fig. 4. Sensitivity and complementary sensitivity functions.

IV. Application Example: Control of a High-Precision Gimbal System

The proposed control architecture is implemented on a high-precision gimbal system given in which is an official product of ASELSAN, Inc. [22]. The goal is to keep the camera's line-of-sight fixed despite all the motion, vibration, and disturbances. The stable nonminimum phase nominal plant that satisfies Assumptions 1, 2, and 5 is

$$P = \alpha_0 \frac{s + 12.3}{s^4 + 841s^3 + 3 \times 10^5 s^2 + 3.8 \times 10^6 s + 1.79 \times 10^7}$$

where $\alpha_0 = 1.8 \times 10^6$, satisfying Assumption 4. This model was obtained from experimental data using N4SID subspace system identification [23]. The input is the motor torque, the output is the gyro signal for the elevation axis. Next, the maximum variation of the nominal plant is obtained, for which the system identification process is carried numerous times for different initial conditions, resulting in $W_T(s) = 2(s + 40)/(s + 210)$. The performance requirements defines that disturbance rejection up to 160 rad/s is required, the maximum possible disturbance imposed is 20 dB at 60 rad/s and closed-loop bandwidth requirement is 165 rad/s. To meet these requirements, the weights used for designing $K_{\rm obs}$ are

$$W_P(s) = \left[\frac{s/\sqrt[k_p]{M_p} + \omega_b}{s + \omega_b \sqrt[k_p]{\epsilon}}\right]^{k_p}, \quad W_{U,\rm obs}(s) = \left[\frac{s + \omega_u/\sqrt[k_u]{M_u}}{s\sqrt[k_u]{\epsilon} + \omega_u}\right]^{k_u}$$

where $\omega_b = 2\pi\,60$ rad/s is the cutoff frequency for $S_{\rm obs}$, $M_p = 1$ limits its gain to unity (thus no overshoot), $\omega_u = 2\pi\,90$ rad/s is the cutoff frequency for $K_{\rm obs}S_{\rm obs}$, $M_U = 500$ limits its gain, $k_p = 1$, $k_u = 7$ are filter degrees, and $\epsilon = 0.0001$ achieves approximate integral action. Following the procedure in Section III-A, a solution was obtained with $\gamma_{\rm opt} = 0.95$, which is close to the limit performance and $S_{\rm obs}$ being very close to the weight W_P. Next, an ISMC is designed using the rules in Sections III-B and III-C, followed by some experimental tuning. As a result, the gain k_0/α_0 and λ are chosen as 1.75 and 20, respectively. For practical implementation derivative filtering is utilized and the signum function is replaced with saturation. The sensitivity/complementary sensitivity functions of the nominal system and the D/UE are shown in Fig. 4. Since a quasi-linear representation is utilized for K, multiple lines appear for S and T. Each line corresponds to one of the ten equally spaced values in the range $A^* \in (0, 15)$. The upper bound is chosen to cover, with some safety margin, the highest amount of uncertainty anticipated. The frequency response can be thought to lie within the bounds of the family of lines seen in the figure. Fig. 5 shows the control effort in comparison to what would happen without the D/UE. First case is the control structure with no D/UE and sgn being used for ISMC. Second is with no D/UE but sgn replaced by sat. Third is the proposed structure with D/UE and sat. The results support the claims in Remark 4. The RS and robust performance conditions as defined by Theorems 4 and 5 are shown in Fig. 6 for the system with and without the D/UE. It is seen that robust performance is achieved for the DOBC case, but the condition is not met without the D/UE.

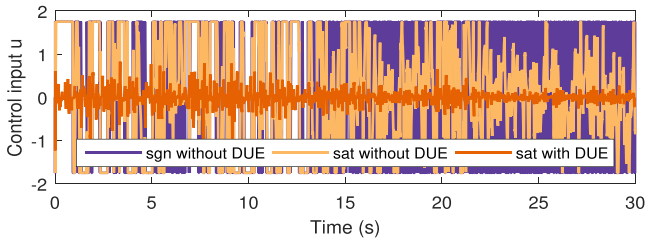

Fig. 5. Control input signal for different cases.

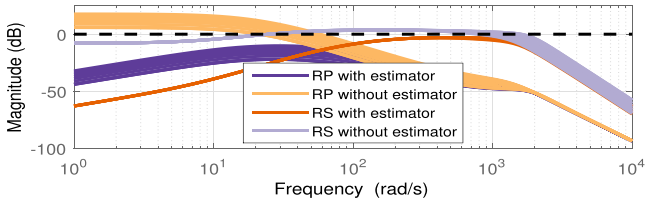

Fig. 6. Comparison of the RS/performance criteria with/without the D/UE.

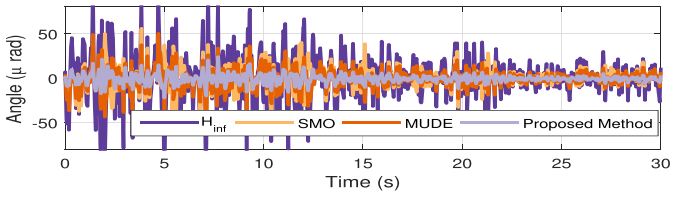

Fig. 7. Angular displacement comparison (experimental).

To benchmark the proposed method, a comparison is made with the case when both $K_{\rm obs}$ and K are designed via $\mathcal{H}_\infty$-synthesis, instead of K being designed with ISMC. Moreover, comparisons are also made with two other state-of-the-art techniques, namely sliding-mode observer (SMO) [24] and MUDE [13]. All methods were run with various parameter variations and those resulting in the best performance were selected for presentation here. The form of the SMO is

$$\dot{z}(t) = Az(t) + Bu(t) - G_l e_y(t) + G_n \vartheta$$

where $\vartheta = -\rho(t, y, u) P_0 e_y / \|P_0 e_y\|, e_y(t) := Cz(t) - y(t)$ is the estimation error, P_0 is a symmetric positive definite matrix, and the scalar function $\rho(.)$ is the design parameter. The form of the MUDE is

$$U(s) = B^+ (A_m X + B_m C - AX) - B^+ K_e E + \text{UDE}$$

where $\text{UDE} := B^+ [(A - sI)X(s) + BU(s)e^{-\tau s}] G_f(s)$. Here, we take $\tau = 0$ since the system is minimum-phase. Fig. 7 shows the angular displacement of the gimbal, which is a standard measure of gimbal performance in vision applications, under the same environmental condition for all methods considered. The proposed method also seems to improve upon SMO and MUDE. The figure actually shows the worst case performance for the proposed approach; the experiments were repeated numerous time for different initial conditions. It was observed for all experiments that the proposed approach remains stable with acceptable performance, hence supporting Theorems 3–5 experimentally. The usefulness of the ISMC controller as the main controller is also evident: The displacement is considerably higher when an $\mathcal{H}_\infty$-based main controller is utilized.

As an extra comparison in Fig. 8 simulation results are presented to evaluate only the D/UE parts. For simplicity, we focus only on disturbance estimation so the nominal model is used without uncertainty. In the top subplot, the disturbance is a swept sine function, where all methods provide good estimates. Note that by design, the proposed approach gradually reduces its estimate outside the observer bandwidth, as expected from Lemma 2 and Theorem 1. This could be useful in avoiding unwanted high-frequency estimation (e.g., noises). Phase shift is also more at higher frequencies as seen inside the zoom-window. Reducing the gain at high phase shift could help improve stability characteristics. Doing so, however, some residual disturbance remains at high frequencies. In the proposed method, these are tackled by the ISMC. In this sense, the $\mathcal{H}_\infty$-based D/UE and the ISMC-based main controller complement each other. The bottom subplot of Fig. 8 shows the estimation under a custom disturbance profile. Once again all methods perform as desired. Note that the proposed method has no overshoot and it displays low settling time. It is straightforward to set such properties in the proposed method through shaping $T_{\rm obs}$ as described in Remark 2.

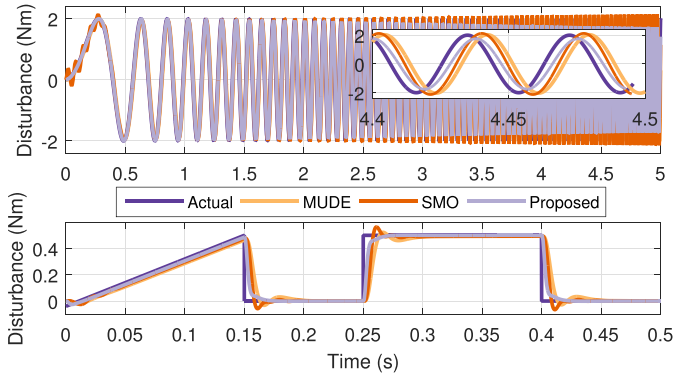

Fig. 8. Disturbance estimation comparison (simulation).

V. Conclusion

A novel D/UE-based ISMC approach is proposed. Explicit expressions for RS, performance, and bandwidth were derived, which had been proposed as open problems for DOBC systems. Common industrial requirements are satisfied by the ISMC, whose quasi-linear representation enables integration into robustness analysis. Experimental and simulation results confirm that the proposed method performs well in comparison to state-of-the-art DOBC methods.

References

[1] S. V. Emelyanov, "A technique to develop complex control equations by using only the error signal of control variable and its first derivative." *Avtomatika i telemekhanika*, vol. 18, no. 10, pp. 873–885, 1957.
[2] V. Utkin, "Survey paper variable structure systems with sliding modes," *IEEE Trans. Automat. Control*, vol. AC-22, no. 2, pp. 212–222, Apr. 1977.
[3] V. Utkin and J. Shi, "Integral sliding mode in systems operating under uncertainty conditions," in *Proc. 35th IEEE Conf. Decis. Control*. IEEE, 1996, vol. 4, pp. 4591–4596.
[4] M. L. Corradini and G. Orlando, "Linear unstable plants with saturating actuators: robust stabilization by a time varying sliding surface," *Automatica*, vol. 43, no. 1, pp. 88–94, 2007.
[5] M. Yan and Y. Shi, "Robust discrete-time sliding mode control for uncertain systems with time-varying state delay," *IET Control Theory Appl.*, vol. 2, no. 8, pp. 662–674, 2008.
[6] C. Edwards, A. Akoachere, and S. K. Spurgeon, "Sliding-mode output feedback controller design using linear matrix inequalities," *IEEE Trans. Automat. Control*, vol. 46, no. 1, pp. 115–119, Jan. 2001.
[7] C. Edwards and S. K. Spurgeon, *Sliding Mode Control: Theory and Applications*. Boca Raton, FL, USA: CRC Press, 1998.

[8] X. Yu and O. Kaynak, "Sliding-mode control with soft computing: A survey," *IEEE Trans. Ind. Electron.*, vol. 56, no. 9, pp. 3275–3285, Sep. 2009.
[9] S. Li, H. Sun, J. Yang, and X. Yu, "Continuous finite-time output regulation for disturbed systems under mismatching condition," *IEEE Trans. Automat. Control*, vol. 60, no. 1, pp. 277–282, Jan. 2015.
[10] X. Wang, S. Li, X. Yu, and J. Yang, "Distributed active anti-disturbance consensus for leader-follower higher-order multi-agent systems with mismatched disturbances," *IEEE Trans. Automat. Control*, vol. 62, no. 11, pp. 5795–5801, Nov. 2017.
[11] H. H. Choi, "LMI-based sliding surface design for integral sliding mode control of mismatched uncertain systems," *IEEE Trans. Automat. Control*, vol. 52, no. 4, pp. 736–742, Apr. 2007.
[12] W.-H. Chen, "Nonlinear disturbance observer-enhanced dynamic inversion control of missiles," *J. Guid., Control, Dyn.*, vol. 26, no. 1, pp. 161–166, 2003.
[13] L. Sun, D. Li, Q.-C. Zhong, and K. Y. Lee, "Control of a class of industrial processes with time delay based on a modified uncertainty and disturbance estimator," *IEEE Trans. Ind. Electron.*, vol. 63, no. 11, pp. 7018–7028, Nov. 2016.
[14] J. Yang, S. Li, and X. Yu, "Sliding-mode control for systems with mismatched uncertainties via a disturbance observer," *IEEE Trans. Ind. Electron.*, vol. 60, no. 1, pp. 160–169, Jan. 2013.
[15] D. Ginoya, P. Shendge, and S. Phadke, "Sliding mode control for mismatched uncertain systems using an extended disturbance observer," *IEEE Trans. Ind. Electron.*, vol. 4, no. 61, pp. 1983–1992, Apr. 2014.
[16] J. Zhang, X. Liu, Y. Xia, Z. Zuo, and Y. Wang, "Disturbance observer based integral sliding mode control for systems with mismatched disturbances," *IEEE Trans. Ind. Electron.*, vol. 63, no. 11, pp. 7040–7048, Nov. 2016.
[17] W.-H. Chen, J. Yang, L. Guo, and S. Li, "Disturbance-observer-based control and related Methods—An overview," *IEEE Trans. Ind. Electron.*, vol. 63, no. 2, pp. 1083–1095, Feb. 2016.
[18] J.-H. She, M. Fang, Y. Ohyama, H. Hashimoto, and M. Wu, "Improving disturbance-rejection performance based on an equivalent-input-disturbance approach," *IEEE Trans. Ind. Electron.*, vol. 55, no. 1, pp. 380–389, Jan. 2008.
[19] J. C. Doyle, B. A. Francis, and A. R. Tannenbaum, *Feedback Control Theory*. North Chelmsford, MA, USA: Courier Corporation, 2013.
[20] A. Levant, "Higher-order sliding modes, differentiation and output-feedback control," *Int. J. Control*, vol. 76, no. 9/10, pp. 924–941, 2003.
[21] J.-J. E. Slotine and W. Li, *Applied Nonlinear Control*. Englewood Cliffs, NJ, USA: Prentice-Hall, 1991.
[22] B. Kürkçü and C. Kasnakoğlu, "Estimation of unknown disturbances in gimbal systems," *Appl. Mech. Mater.*, vol. 789, pp. 951–956, 2015.
[23] P. Van Overschee and B. De Moor, "N4SID: Subspace algorithms for the identification of combined deterministic-stochastic systems," *Automatica*, vol. 30, no. 1, pp. 75–93, 1994.
[24] C. Edwards, S. K. Spurgeon, and R. J. Patton, "Sliding mode observers for fault detection and isolation," *Automatica*, vol. 36, no. 4, pp. 541–553, 2000.